Umklapp Superradiance with a Collisionless Quantum Degenerate Fermi Gas

Francesco Piazza[1,*] and Philipp Strack[2]
[1]Physik Department, Technische Universität München, 85747 Garching, Germany
[2]Department of Physics, Harvard University, Cambridge, Massachusetts 02138, USA
(Received 11 September 2013; published 8 April 2014)

The quantum dynamics of the electromagnetic light mode of an optical cavity filled with a coherently driven Fermi gas of ultracold atoms strongly depends on the geometry of the Fermi surface. Superradiant light generation and self-organization of the atoms can be achieved at low pumping threshold due to resonant atom-photon umklapp processes, where the fermions are scattered from one side of the Fermi surface to the other by exchanging photon momenta. The cavity spectrum exhibits sidebands that, despite strong atom-light coupling and cavity decay, retain narrow linewidth, due to absorptionless transparency windows outside the atomic particle-hole continuum and the suppression of broadening and thermal fluctuations in the collisionless Fermi gas.

DOI: 10.1103/PhysRevLett.112.143003 PACS numbers: 37.30.+i, 03.75.Ss, 42.50.Pq

Introduction.—Lasing [1,2] and superradiance phenomena are currently enjoying a renaissance as research topics in atomic physics. Recent advances in quantum optical experiments with ultracold atoms enable the exploration of a new regime at ultralow temperatures in which quantum effects of both the light and the atomic matter field become important, atoms and confined photon fields are strongly coupled, and the photon field is actually dynamical, playing a much more active role than in optical lattice experiments.

In many-body cavity quantum electrodynamics, where many ultracold atoms are placed in an optical resonator [3], the role of the photon is dual. First, it mediates an interaction between the atoms producing new phases of matter, whose dynamics, in turn, backacts on the photon field itself. Second, the photon output serves as a noninvasive probe of optical properties such as refraction and absorption of the underlying atomic medium.

An important question is in how far favorable coherence properties of the atomic medium can be imprinted onto the light field. To that end, a recent string of experiments has achieved superradiance [4] in which the N atoms *collectively* interact with the light field: with Raman photons [5,6], with momentum recoil in thermal and condensed Bose gases [7–13], and with photon gases in optical cavities [14,15]. In related superradiant lasers [16–20], the emitted intensity can be amplified $\sim N^2$ while there is substantial $\sim 1/N^2$ linewidth narrowing, with potential technological applications for precision spectroscopy and quantum metrology.

The purpose of this Letter is to pin down the consequences of the Fermi surface in many-fermion cavity quantum electrodynamics not available with the previously discussed bosons or (effective) spins [21–47]. Motivated by near-time experimental prospects to study superradiant phenomena with fermionic atoms in a transversally driven optical cavity (sketched in Fig. 1), we here provide a computation of the steady-state phase diagrams for one- and two-dimensional confinement of the Fermi gas as well as the cavity spectrum for this system. Single-spin fermions are appealing as a coherent optical medium since frequency shifts from collisions are strongly suppressed, a feature also exploited in optical clocks [48–50]. Optomechanics with fermions was considered previously in Refs. [51,52], and glassy fermions in multimode cavities were discussed in Ref. [53].

Key results.—The Fermi gas is generically closer to superradiance threshold due to umklapp scattering events between points on the Fermi surface transferring the two-photon momentum $\mathbf{Q}$ at no energy cost. The density and the confinement dimensionality of the Fermi gas drastically affect available phase space volume for low energy umklapp processes. Atomic self-organization, concomitant with superradiance, occurs here as a dynamical Peierls instability without a preformed, conservative lattice potential parallel to the cavity axis. In $d = 1$, perfect nesting between $\mathbf{Q}$ and $\mathbf{k}_F$ strongly reduces the critical pump strength towards a fermionic superradiant state, which can

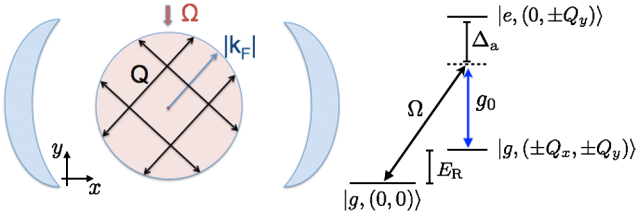

FIG. 1 (color online). Left: Fermi sphere (red circle) of the ultracold, atomic Fermi gas inside the mirrors of an optical cavity (curved, blue) in combined position-momentum representation. $|\mathbf{k}_F|$ is the Fermi momentum and $\mathbf{Q}$ is the superposition of the cavity momentum and the momentum of coherent drive laser with amplitude Ω. Right: Level scheme employed for the superradiant self-organization discussed here, with single-photon atom-cavity Rabi coupling g_0. Generalizing the level structure above to an incoherent repumping scheme should enable superradiant umklapp lasing [18–20].

become fully insulating. In $d = 2$, cavity-mediated Fermi surface reconstruction leads to "pockets" of gapless excitations similar to magnetic metals [54].

The cavity spectrum, instead of the usual broadened polaritonic peaks, shows a broad continuum with sharp edges plus two perfectly narrow sidebands shown in Fig. 2. Sufficiently close to the self-organization transition, the sidebands appear in "absorptionless" transparency windows (below $\omega/E_R \lesssim 0.6$), and as such they remain perfectly sharp. The underlying absorption and refractive properties of the coherent atomic Fermi medium, shown in Fig. 3, are determined by the imaginary and real parts of the particle-hole continuum, respectively. Moreover, we expect the sidebands to be robust against thermal noise, due to the absence of collisions in the single-spin Fermi gas and the associated reduced sensitivity to thermal fluctuations (especially in interacting Bose superfluids, order parameter fluctuations will strongly deplete the condensate fraction available for recoil lasing); the far detuning between the internal atomic transition and the cavity frequency also ensures that decay from the excited atomic state is suppressed. Currently used Fabry-Perot cavities with MHz decay rates are in the bad-cavity limit compared to the "slow motion" of alkali atoms with kHz kinetic energies, leading to a decoupling of the photon decay and the collective dynamics of the atoms [12,13,19,20]. Indeed, our results here are confirmed in a nonequilibrium calculation [55].

Setup and formalism.—We consider N spinless fermionic atoms with two internal electronic levels in the setup of Fig. 1. The quantized excitations of the coupled atoms plus driven cavity system will be described in terms of the field operators $\hat{\psi}_{g|e}$ for the atoms in the internal ground or excited state and the annihilation operator $\hat{a}$ for a cavity photon [31]. The atomic operators obey fermionic quantum statistics and fulfill the (anti)commutation relation $\{\hat{\psi}(\mathbf{r}), \hat{\psi}^\dagger(\mathbf{r}')\} = \delta_{\mathbf{r},\mathbf{r}'}$. In a frame rotating with the frequency ω_p of the pump laser, the Hamiltonian $\hat{H} = \hat{H}_a + \hat{H}_c + \hat{H}_{a|c} + \hat{H}_{a|p}$ contains four terms: $\hat{H}_c = -\Delta_c \hat{a}^\dagger \hat{a}$ and

$$\begin{aligned}
\hat{H}_a &= -\int d\mathbf{r}\left[\hat{\psi}_g^\dagger(\mathbf{r})\left(\frac{\nabla^2}{2m}\right)\hat{\psi}_g(\mathbf{r})\right. \\
&\quad \left. + \hat{\psi}_e^\dagger(\mathbf{r})\left(\frac{\nabla^2}{2m} + \Delta_a\right)\hat{\psi}_e(\mathbf{r})\right], \\
\hat{H}_{a|c} &= -ig_0 \int d\mathbf{r}\hat{\psi}_g^\dagger(\mathbf{r})\eta_c(\mathbf{r})\hat{a}^\dagger\hat{\psi}_e(\mathbf{r}) + \text{H.c.}, \\
\hat{H}_{a|p} &= -i\Omega \int d\mathbf{r}\hat{\psi}_g^\dagger(\mathbf{r})\eta_p(\mathbf{r})\hat{\psi}_e(\mathbf{r}) + \text{H.c.} \qquad (1)
\end{aligned}$$

Here, $\hat{H}_a$ describes the kinetic energy of the atoms with mass m moving around inside the cavity, with the excited state detuning between the pump and the atomic resonance $\Delta_a = \omega_p - \omega_c$. $\Delta_c = \omega_p - \omega_c$ is the detuning between the pump and the cavity mode and Ω is the pump Rabi frequency. We operate in the standard regime where the atoms couple to only a single excitation mode of the electromagnetic field of the cavity with single-photon Rabi coupling g_0. The functions $\eta_c(\mathbf{r}) = \cos(\mathbf{Q}_c \cdot \mathbf{r})$ and $\eta_p(\mathbf{r}) = \cos(\mathbf{Q}_p \cdot \mathbf{r})$ [we choose $\mathbf{Q}_{c(p)} = Q_{x(y)}\hat{\mathbf{x}}(\hat{\mathbf{y}})$ below] contain the spatial structure of the mode functions of the (standing-wave) cavity light field and the pump laser, respectively.

We extend our recently developed effective action formalism [57] to fermionic quantum fields and to situations with a spatially varying pump laser potential. We neglect the spontaneous emission from the excited atomic level by assuming that the detuning Δ_a be by far the largest energy scale such that population of the excited level is suppressed. This allows us to adiabatically eliminate the excited atomic level and derive an effective action for the low-lying levels coupled to the cavity (see Supplemental Material [60]). The effective action is amendable to a saddle-point analysis at

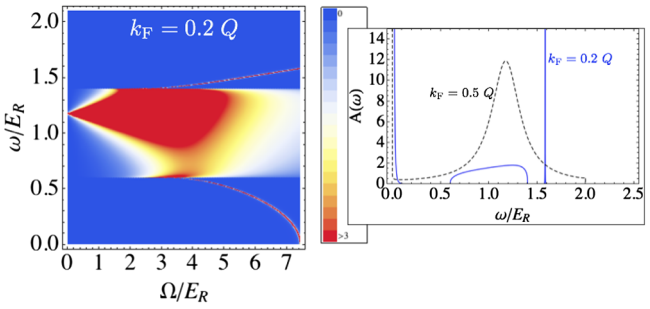

FIG. 2 (color online). Cavity photon spectrum in one dimension. Left: Spectral function Eq. (2) in color scale. The narrow features are actually sharp δ-function peaks, the lower of which moves toward $\omega = 0$ for $\Omega \to \Omega_D$. Right: Spectral function at fixed coupling close to threshold, $\Omega = 0.98\Omega_D$, for two different densities. Black dashed curve: Perfectly nested case in which the fermionic particle-hole continuum reaches down to zero frequency and $\Omega_D = 0$. Parameters are $\Delta_c = -1.2E_R$, $Ng_0^2/\Delta_a = -0.05E_R$, $g_0/\Delta_a = -0.1E_R$, $T = 0$. Within the particle-hole continuum there is "broadband" emission for a range of frequencies; outside of the particle-hole continuum, the linewidth remains narrow.

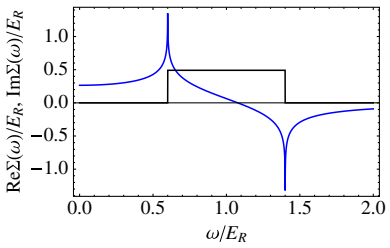

FIG. 3 (color online). Absorption (imaginary part of the particle-hole continuum, black box-shaped line) and refractive properties (real part of the particle-hole continuum, blue double-peaked line) of the coherent atomic Fermi medium in one dimension at $\Omega = 0.6\Omega_D$. The lower sideband in Fig. 2 appears in the absorptionless "transparency window" for $\omega/E_R \lesssim 0.6$, for which the imaginary part is identically zero since here $k_F = 0.2Q$ is away from perfect nesting. At perfect nesting $Q = 2k_F$, the absorption reaches to $\omega = 0$. The optical properties of the atomic Fermi medium can be tuned by the coherent drive Ω highlighting connections to electromagnetically induced transparency [56].

fixed density $n_\psi = N/L^d$, as done in Ref. [57]. The corresponding mean-field solution $\alpha = \langle \hat{a} \rangle$ becomes exact in the thermodynamic limit $N, L \to \infty$, $n_\psi = \text{const}$, yielding the phase diagram as a function of the pump strength Ω, the fermion density n_ψ, dimensionality d, and temperature T.

Self-organization for 1D confinement.—The phase diagram for the $d = 1$ case, when the fermionic atoms are tightly confined in tubes parallel to the cavity axis so that the two-photon momentum transfer $\mathbf{Q} = \mathbf{Q}_c + \mathbf{Q}_p \simeq \mathbf{Q}_c$, is shown in Fig. 4. The critical pump strength Ω_D, above which the system is self-organized or superradiant, strongly depends on the fermion density or, equivalently, on the 1D Fermi momentum $k_F^{1D} = \pi n_\psi$. In particular, we notice a strong suppression of Ω_D when $k_F^{1D} \simeq Q/2$. This condition indeed implies that a cavity photon can scatter an atom from the Fermi surface (for $d = 1$ Fermi points) at very low energy cost with a momentum transfer $\mathbf{Q}$ which inverts the direction of the atomic motion (umklapp scattering). For fermions in $d = 1$, the system becomes unstable towards superradiance even at infinitesimal pump strength for $T = 0$ and $k_F^{1D} = Q/2$. The $T = 0$ line in Fig. 4 goes indeed to zero like $1/\ln|1 - Q/2k_F|^{-1}$, while as soon as a small finite temperature (also potentially induced by cavity decay) is present, Ω_D stays finite. This is analogous to the Peierls instability present in one-dimensional metals [58], where it becomes energetically favorable for the electrons to break the discrete translational symmetry by doubling the lattice period so that the Fermi points get gapped out, with the important difference that here the cavity generated lattice does not reorganize but rather first appears due to the instability. Reference [59] is a related proposal to simulate Peierls physics with hybrid ultracold atom and ion systems. Our system becomes insulating in the superradiant phase for nearly commensurate densities $k_F^{1D} \simeq jQ/2$ (with j integer), as is shown for $j = 1, 2$ in Fig. 4. The superradiant Peierls insulating regions are separated by crossover lines from regions where the system shows superradiant charge order but is still metallic, since the Fermi energy does not lie within the band gap. In addition to measurements of the cavity spectrum (see also below), the superradiant Peierls insulator (SPI) and superradiant charge ordered Fermi liquid (SCOFL) phases could be distinguished by radio frequency spectroscopy of the atomic cloud. The Fermi liquid (FL)-SCOFL transition is always continuous except from a region around $k_F \simeq Q$, where the transition is first order. The red shaded area in Fig. 4 shows the region where the free energy has two local minima as a function of the order parameter α. This hysteresis region appears for Ω slightly lower than Ω_D and ends exactly at Ω_D, where the free energy has only a single minimum at finite α, corresponding to the jump in the cavity occupation. Since the atoms couple to a single cavity mode extending all over the cloud, there is no coexistence between the normal and superradiant phase despite hysteresis.

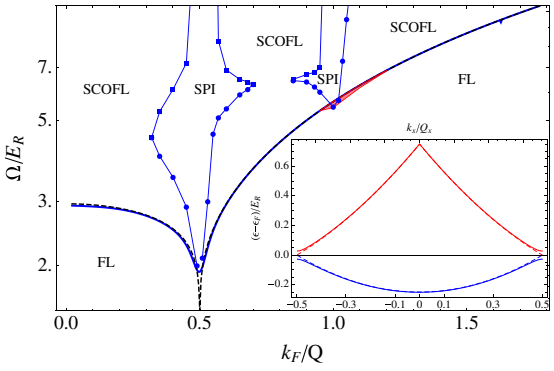

FIG. 4 (color online). Phase diagram for a one-dimensional Fermi gas in an optical cavity as a function of Fermi (k_F) over cavity ($Q = \sqrt{2mE_R}$) momentum versus pump amplitude Ω. Inset shows gap opening at the Fermi points. Temperatures are $k_B T = 0$ (black dashed line), $k_B T = 0.01 E_R$ (blue solid line). At $Q = 2k_F$ the system is perfectly nested and Peierls reconstruction into a superradiant Peierls insulator (SPI) sets in at relatively small Ω. Away from nesting the Z_2 charge symmetry breaking leads to a superradiant charge-ordered Fermi liquid (SCOFL). The red shaded area extending from the second-order transition line indicates the hysteresis region preceding the first-order phase transition from the Fermi liquid (FL) into the the SPI at $k_F/Q = 1$; there the Fermi energy lies in the gap between the second and third cavity generated bands. The remaining parameters are $\Delta_c = -0.2E_R$, $Ng_0^2/\Delta_a = -0.05E_R$, $g_0/\Delta_a = -0.1$.

Self-organization for 2 D confinement.—In two dimensions the physics is richer since the spatial structure of the pump laser cannot be neglected. This has two main effects: (i) even in the normal phase, by increasing the pump strength we deform the Fermi surface of the atoms inside the pump lattice with vector $\mathbf{Q}_p$, and (ii) the density wave in the superradiant phase has momentum $\mathbf{Q} = \mathbf{Q}_c + \mathbf{Q}_p$, corresponding to a checkerboard lattice with reciprocal vector $\mathbf{Q}$ whose length is $Q = \sqrt{Q_x^2 + Q_y^2}$ [60]. The phase diagram for different temperatures as a function of the Fermi momentum along the $\mathbf{Q}$ direction (the relevant nesting direction) calculated at the critical pump strength $k_{F,\hat{\mathbf{Q}}}(\Omega_D)$ is presented in Fig. 5. As in the $d = 1$ case, we observe a suppression of Ω_D for $k_{F,\hat{\mathbf{Q}}}(\Omega_D) \simeq Q/2$, marked by the vertical black dashed line in Fig. 5. The suppression of Ω_D is much weaker as compared to $d = 1$ since perfect nesting is absent. Again, the minimum in Ω_D is at $k_{F,\hat{\mathbf{Q}}}(\Omega_D) \simeq Q/2$, where this time the Fermi momentum depends on the pump strength due to the deformation of the Fermi surface discussed in (i). In Fig. 5, the minimum is not exactly at $k_{F,\hat{\mathbf{Q}}}(\Omega_D) = Q/2$ since $T \neq 0$. In addition, the self-organization transition in $d = 2$ can correspond to reconstruction of the Fermi surface for $k_{F,\hat{\mathbf{Q}}}(\Omega_D) > Q/2$, an example of which is given in the upper right-hand inset of Fig. 5. By entering the self-organized phase, the atoms change from a simply connected Fermi surface to one consisting of separated closed surfaces delimiting zones with occupied and empty states. The blue square-shaped Fermi surface belongs to the first checkerboard lattice band, while the red star-shaped surface belongs to the second

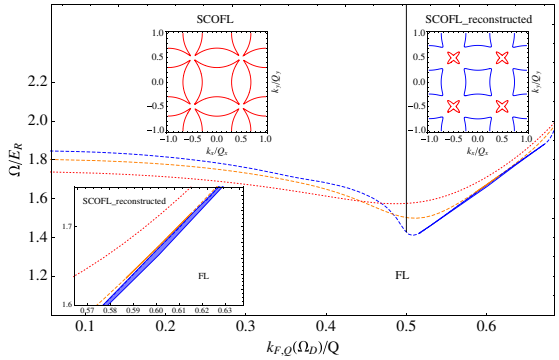

FIG. 5 (color online). Phase diagram for a two-dimensional Fermi gas in an optical cavity for $Q_x = Q_y = \sqrt{2mE_R}$, $k_BT = 0.01E_R$ (blue dashed line), $k_BT = 0.05E_R$ (orange dashed line), and $k_BT = 0.1E_R$ (red dotted line). Lower inset: Hysteresis region. The vertical line separates the two different superradiant regimes with topologically trivial Fermi surface and reconstructed Fermi surface, as illustrated in the two upper insets: left at $k_{F,\hat{\mathbf{Q}}}(\Omega_D) = 0.49Q$, $\alpha = 0.1$, right at $k_{F,\hat{\mathbf{Q}}}(\Omega_D) = 0.53Q$, $\alpha = 0.2$. Here the Fermi surface is shown in the repeated-zone scheme relative to the Brillouin zone $\mathcal{B} = (-Q_x/2 < k_x < Q_x/2, -Q_y/2 < k_y < Q_y/2)$. Purple lines delimit "electron" pockets with occupied levels while blue lines delimit hole pockets with empty levels. The vertical line separating the two superradiant phases is straight only close to Ω_D. The remaining parameters are as in Fig. 4.

higher band. The condition $k_{F,\hat{\mathbf{Q}}}(\Omega_D) > Q/2$ implies that the Fermi surface has to intersect the first Bragg plane of the reciprocal checkerboard lattice [60]. These phases with different Fermi surface topologies could be distinguished by time-of-flight imaging of the atomic cloud.

In contrast to the one-dimensional case, in $d = 2$ the atomic medium is, therefore, always metallic in the superradiant phase. The order of the superradiant transition depends on $k_{F,\hat{\mathbf{Q}}}(\Omega_D)$ and temperature. As can be seen from Fig. 5, there is a large region where the transition is first order and hysteresis is present (indicated by the shaded area). The range of densities for which the transition is first order gets smaller with increasing temperature (see lower inset in Fig. 5). In $d = 2$, the Fermi momentum at $\Omega = 0$ reads $|\mathbf{k}_F^{2D}| = \sqrt{4\pi n_\psi}$ and the cavity momentum is $Q_x = 2\pi/\lambda$, with λ an optical wavelength, for example, ~800 nm. For a degenerate Fermi gas at densities around 10^{14}–10^{15} m^{-2}, the various regimes discussed here are thus experimentally accessible.

Cavity spectrum for 1 D confinement.—We now turn to the cavity spectrum (shown above in Fig. 2), which is as well dramatically affected by the presence of a sharp Fermi surface at low T. The cavity spectral function,

$$A(\omega) = \frac{-2(\delta_c + \omega)^2 \mathrm{Im}\Sigma(\omega)}{[\delta_c^2 - \omega^2 + 2\delta_c \mathrm{Re}\Sigma(\omega)]^2 + [2\delta_c \mathrm{Im}\Sigma(\omega)]^2}, \quad (2)$$

with the shifted cavity detuning $\delta_c = -\Delta_c + Ng_0^2/2\Delta_a$, describes how the spectral weight is distributed between different frequencies under a weak probe but, being normalized to 2π, does not contain information about the intensity. The function $\Sigma(\omega) = -(\lambda^2/2n)\Pi_F(\omega, \mathbf{Q})$ (shown in Fig. 3) describes how a photon is dressed by atomic fluctuations: its real part shifts the photon frequency while its imaginary part gives rise to broadening. Here, $\lambda = \Omega g_0/\Delta_a$. We will focus on the zero temperature case. Explicit formulas for the particle-hole polarization function $\Pi_F(\omega, \mathbf{Q})$ are given in the Supplemental Material [60]. For energies within the particle-hole continuum, $(Q/k_F)^2 - 2Q/k_F \le \omega/\epsilon_F \le (Q/k_F)^2 + 2Q/k_F$, the broadening of the photon spectrum is determined by a frequency-independent constant

$$\mathrm{Im}\Sigma(\omega)_{1\mathrm{D}} = -\frac{\lambda^2 \pi k_F}{8\epsilon_F Q}. \quad (3)$$

This broadening ("Landau damping") arises from real scattering events between photon and atom where momentum and energy are conserved $\omega = \epsilon_{k+Q} - \epsilon_k$. Instead of normal-mode split polariton peaks in the cavity spectrum [with $A(\omega)$ being the sum of two Lorentzians], Fig. 2 exhibits a broad feature disappearing with a discontinuity for frequencies out of the particle-hole continuum, where $\mathrm{Im}\Sigma(\omega) = 0$. Moreover, when the particle-hole fluctuations in the atomic medium shift [through $\mathrm{Re}\Sigma(\omega)$] the cavity frequency outside the particle-hole continuum, the cavity spectrum shows sharp sidebands $A(\omega) = [1 + \delta_c \mathrm{Re}\Sigma(\omega = E)]\pi\delta(\omega - E)$. The absence of damping in the low frequency range is due to the Pauli principle, which forbids scattering of a fermion into an occupied state, while in the high frequency range it is due to the sharpness of the Fermi surface, such that suddenly no fermions are available for scattering above a given threshold. In particular, the lower sideband is found at the "soft-mode" energy E, which close to the critical point is $E \simeq \sqrt{\delta_c^2 + 2\delta_c \mathrm{Re}\Sigma(\omega = 0)}$ and goes to zero at the critical pump strength Ω_D. Close to perfect nesting $Q = 2k_F$, see the right-hand panel of Fig. 2, the broad spectral feature reaches down to $\omega = 0$, leaving no space for a sharp soft mode.

Summary.—We considered the optical properties and self-organization of a coherently driven Fermi gas strongly coupled to the light field of an optical resonator. New Fermi surface physics leads to superradiance and self-organization at low pumping threshold as well as the appearance of narrow sidebands in the cavity spectrum. Generalizations of this work could lead to superradiant umklapp lasers as well as new nonequilibrium phases of interacting fermions.

We are grateful to W. Zwerger for collaboration and guidance on related work, and to M. D. Lukin and H. Ritsch for insightful discussions and references on lasing. This work was supported by the Alexander Von Humboldt foundation, the DFG under Grant No. Str 1176/1-1, the NSF under Grant No. DMR-1103860, the Templeton foundation, the Center for Ultracold Atoms (CUA), and the Multidisciplinary University Research Initiative (MURI).

Note added.—Recently, two other works addressing a similar problem appeared [61,62].

*Corresponding author.
francesco.piazza@ph.tum.de

[1] A. E. Siegman, *Lasers* (University Science Books, Mill Valley, 1986).
[2] H. Haken, *Light*, Laser Light Dynamics Vol. 2 (North-Holland, Amsterdam, 1985).
[3] H. Ritsch, P. Domokos, F. Brennecke, and T. Esslinger, Rev. Mod. Phys. **85**, 553 (2013).
[4] R. H. Dicke, Phys. Rev. **93**, 99 (1954).
[5] S. Inouye *et al.*, Science **285**, 571 (1999).
[6] Y. Yoshikawa, Y. Torii, and T. Kuga, Phys. Rev. Lett. **94**, 083602 (2005).
[7] A. T. Black, H. W. Chan, and V. Vuletić, Phys. Rev. Lett. **91**, 203001 (2003).
[8] S. Slama, S. Bux, G. Krenz, C. Zimmermann, and P. W. Courteille, Phys. Rev. Lett. **98**, 053603 (2007).
[9] K. J. Arnold, M. P. Baden, and M. D. Barrett, Phys. Rev. Lett. **109**, 153002 (2012).
[10] K. Baumann, C. Guerlin, F. Brennecke, and T. Esslinger, Nature (London) **464**, 1301 (2010).
[11] K. Baumann, R. Mottl, F. Brennecke, and T. Esslinger, Phys. Rev. Lett. **107**, 140402 (2011).
[12] R. Mottl, F. Brennecke, K. Baumann, R. Landig, T. Donner, and T. Esslinger, Science **336**, 1570 (2012).
[13] F. Brenneke, R. Mottl, K. Baumann, R. Landig, T. Donner, and T. Esslinger, Proc. Natl. Acad. Sci. U.S.A. **110**, 11 763 (2013).
[14] J. Klaers, J. Schmitt, F. Vewinger, and M. Weitz, Nature (London) **468**, 545 (2010).
[15] M. Weitz, J. Klaers, and F. Vewinger, Phys. Rev. A **88**, 045601 (2013).
[16] M. Gross and S. Haroche, Phys. Rep. **93**, 301 (1982).
[17] Y. Yamamoto and A. Imamoglu, *Mesoscopic Quantum Optics* (Wiley & Sons, New York, 1999).
[18] F. Haake, M. I. Kolobov, C. Fabre, E. Giacobino, and S. Reynaud, Phys. Rev. Lett. **71**, 995 (1993).
[19] D. Meiser, J. Ye, D. R. Carlson, and M. J. Holland, Phys. Rev. Lett. **102**, 163601 (2009).
[20] J. G. Bohnet, Z. Chen, J. M. Weiner, D. Meiser, M. J. Holland, and J. K. Thompson, Nature (London) **78**, 484 (2012).
[21] K. Hepp and E. H. Lieb, Ann. Phys. (N.Y.) **76**, 360 (1973).
[22] Y. K. Wang and F. T. Hioe, Phys. Rev. A **7**, 831 (1973).
[23] R. Bonifacio and L. De Salvo, Nucl. Instrum. Methods Phys. Res., Sect. A **341**, 360 (1994).
[24] P. Domokos and H. Ritsch, Phys. Rev. Lett. **89**, 253003 (2002).
[25] C. Emary and T. Brandes, Phys. Rev. E **67**, 066203 (2003).
[26] N. Lambert, C. Emary, and T. Brandes, Phys. Rev. Lett. **92**, 073602 (2004).
[27] J. K. Asbóth, P. Domokos, H. Ritsch, and A. Vukics, Phys. Rev. A **72**, 053417 (2005).
[28] D. Nagy, J. K. Asbóth, P. Domokos, and H. Ritsch, Europhys. Lett. **74**, 254 (2006).
[29] A. Vukics, C. Maschler, and H. Ritsch, New J. Phys. **9**, 255 (2007).
[30] F. Dimer, B. Estienne, A. S. Parkins, and H. J. Carmichael, Phys. Rev. A **75**, 013804 (2007).
[31] C. Maschler, I. Mekhov, and H. Ritsch, Eur. Phys. J. D **46**, 545 (2008).
[32] D. Nagy, G. Szirmai, and P. Domokos, Eur. Phys. J. D **48**, 127 (2008).
[33] J. Larson and M. Lewenstein, New J. Phys. **11**, 063027 (2009).
[34] D. Nagy, G. Konya, G. Szirmai, and P. Domokos, Phys. Rev. Lett. **104**, 130401 (2010).
[35] S. Gopalakrishnan, B. L. Lev, and P. M. Goldbart, Phys. Rev. A **82**, 043612 (2010).
[36] S. Vidal, G. De Chiara, J. Larson, and G. Morigi, Phys. Rev. A **81**, 043407 (2010).
[37] J. Keeling, M. J. Bhaseen, and B. D. Simons, Phys. Rev. Lett. **105**, 043001 (2010).
[38] A. O. Silver, M. Hohenadler, M. J. Bhaseen, and B. D. Simons, Phys. Rev. A **81**, 023617 (2010).
[39] G. Konya, G. Szirmai, and P. Domokos, Eur. Phys. J. D **65**, 33 (2011).
[40] D. Nagy, G. Szirmai, and P. Domokos, Phys. Rev. A **84**, 043637 (2011).
[41] B. Öztop, M. Bordyuh, O. E. Müstecaplioglu, and H. E. Türeci, New J. Phys. **14**, 085011 (2012).
[42] E. G. Dalla Torre, S. Diehl, M. D. Lukin, S. Sachdev, and P. Strack, Phys. Rev. A **87**, 023831 (2013).
[43] M. J. Bhaseen, J. Mayoh, B. D. Simons, and J. Keeling, Phys. Rev. A **85**, 013817 (2012).
[44] D. E. Chang, J. I. Cirac, and H. J. Kimble, Phys. Rev. Lett. **110**, 113606 (2013).
[45] T. Grießer and H. Ritsch, Phys. Rev. Lett. **111**, 055702 (2013).
[46] Y. Li, L. He, and W. Hofstetter, Phys. Rev. A **87**, 051604 (2013).
[47] B. Oeztop, M. Kulkarni, and H. E. Türeci, Phys. Rev. Lett. **111**, 220408 (2013).
[48] E. L. Hazlett, Y. Zhang, R. W. Stites, K. Gibble, and K. M. O'Hara, Phys. Rev. Lett. **110**, 160801 (2013).
[49] T. Akatsuka, M. Takamoto, and H. Katori, Nat. Phys. **4**, 954 (2008).
[50] M. D. Swallows, M. Bishof, Y. Lin, S. Blatt, M. J. Martin, A. M. Rey, and J. Ye, Science **331**, 1043 (2011).
[51] J. Larson, B. Damski, G. Morigi, and M. Lewenstein, Phys. Rev. Lett. **100**, 050401 (2008).
[52] R. Kanamoto and P. Meystre, Phys. Rev. Lett. **104**, 063601 (2010).
[53] M. Müller, P. Strack, and S. Sachdev, Phys. Rev. A **86**, 023604 (2012).
[54] M. Vojta, Physica (Amsterdam) **481C**, 178 (2012).
[55] F. Piazza and P. Strack (to be published).
[56] M. Fleischhauer, A. Imamoglu, and J. P. Marangos, Rev. Mod. Phys. **77**, 633 (2005).
[57] F. Piazza, P. Strack, and W. Zwerger, Ann. Phys. (Amsterdam) **339**, 135 (2013).
[58] R. E. Peierls, *Quantum Theory of Solids* (Clarendon, Oxford, England, 1955).
[59] U. Bissbort, D. Cocks, A. Negretti, Z. Idziaszek, T. Calarco, F. Schmidt-Kaler, W. Hofstetter, and R. Gerritsma, Phys. Rev. Lett. **111**, 080501 (2013).
[60] See Supplemental Material at http://link.aps.org/supplemental/10.1103/PhysRevLett.112.143003 for some details of the calculations.
[61] J. Keeling, M. J. Bhaseen, and B. D. Simons, preceding Letter, Phys. Rev. Lett. **112**, 143002 (2014).
[62] Y. Chen, Z. Yu, and H. Zhai, following Letter, Phys. Rev. Lett. **112**, 143004 (2014).